

Hall effect and resistivity of oxygen-deficient $\text{YBa}_2\text{Cu}_3\text{O}_{7-\delta}$ thin films

A. Carrington, D. J. C. Walker, A. P. Mackenzie, and J. R. Cooper*

*Interdisciplinary Research Center in Superconductivity, University of Cambridge, Madingley Road,
Cambridge CB3 0HE, United Kingdom*

(Received 15 March 1993; revised manuscript received 3 June 1993)

We report measurements of the *ab*-plane resistivity (ρ) and Hall coefficient (R_H) of crystalline thin films of $\text{YBa}_2\text{Cu}_3\text{O}_{7-\delta}$ ($0.05 \leq \delta \leq 0.53$) from below T_c up to 400 K. In contrast to measurements on sintered samples, and some other recent work on thin films, the residual resistivity of these films (as extrapolated from high temperature) remains low for all δ . As oxygen is removed from the films, ρ increases and $\rho(T)$ develops downward curvature below 300 K. The Hall angle (Θ_H) however, continues to obey the relation, $\cot\Theta_H = AT^2 + B$. As δ increases, the coefficient A decreases while B remains constant. Data for an oxygen-deficient single crystal of $\text{YBa}_2\text{Cu}_3\text{O}_{7-\delta}$ agree well with our film data. Measurements of ρ in the region of the superconducting transition in fields of up to 7 T, applied parallel to the crystallographic *a*, *b*, or *c* axes, are also reported. The well-known "field-induced broadening" of the $\rho(T)$ curves becomes larger as δ is increased. There is evidence for a transition line in the field-temperature plane that has the 4/3-power-law behavior associated with critical fluctuations in the three-dimensional *XY* model.

I. INTRODUCTION

The normal-state and superconducting properties of the high-temperature superconductor $\text{YBa}_2\text{Cu}_3\text{O}_{7-\delta}$ are known to be highly dependent upon the oxygen stoichiometry. The primary effect of removing oxygen is to reduce the hole concentration on the CuO_2 planes. The material is optimally doped (i.e., has the highest transition temperature) with $\delta=0.1$.¹

In some ways $\text{YBa}_2\text{Cu}_3\text{O}_{7-\delta}$ is one of the simpler materials in which to investigate the properties of the underdoped side of the phase diagram because the impurity potentials introduced by oxygen vacancies in the CuO chains (separated from the CuO_2 planes by a BaO layer) can be expected to have less of an effect than, for example, Sr^{2+} ions substituting for La in the layer adjacent to the CuO_2 planes in $\text{La}_{2-x}\text{Sr}_x\text{CuO}_4$. One of the reasons for starting the present work was that in a study of polycrystalline material, Cooper *et al.*² observed a steady change in the Hall coefficient (R_H) and resistivity (ρ) as the oxygen content was changed, but there was a substantial increase in the residual resistivity as oxygen was removed. It was not clear whether this was an intrinsic property of the material or due to grain boundary effects. Furthermore, in polycrystalline samples there is always a possibility of there being a contribution from the *c*-axis resistivity, which is known to increase strongly with δ .³

The slow diffusion rate of oxygen in $\text{YBa}_2\text{Cu}_3\text{O}_{7-\delta}$ (Ref. 4) means that a similar study using single crystals would be time consuming. For this reason we decided to use laser ablated thin films, which x-ray studies had shown to be almost perfectly oriented with the *c* axis perpendicular to the substrate surface.⁵ Another advantage of films is that they can be patterned into a standard geometry suitable for transport measurements, removing the uncertainties arising from contact size and position which can be significant in single-crystal measurements.

Preliminary experiments showed that the oxygen content of these films can be changed reproducibly using annealing times of only a few hours (1–4 h).

In this paper we report measurements of the Hall effect and resistivity from below T_c to 400 K on a series of $\text{YBa}_2\text{Cu}_3\text{O}_{7-\delta}$ films ($0.53 \leq \delta \leq 0.05$). We find that the residual resistivity in these samples stays low even for δ values of 0.53, but many of the other qualitative features of $\rho(T)$ are the same as those observed in sintered samples. Although ρ and $1/R_H$ show pronounced nonlinearity in temperature as the oxygen content is decreased, the cotangent of the Hall angle continues to obey the Anderson⁶ relation

$$\cot\Theta_H = AT^2 + B \quad (1)$$

fairly well. The parameter A in (1) decreases monotonically with increasing δ whereas B remains roughly constant. This variation of parameters A and B is in qualitative agreement with recent results on Co-doped $\text{YBa}_2\text{Cu}_3\text{O}_{7-\delta}$ single crystals,⁷ demonstrating the similarity of doping the CuO chains with either Co atoms or oxygen vacancies. We recently became aware of some other recent studies of oxygen-depletion effects on $\text{YBa}_2\text{Cu}_3\text{O}_{7-\delta}$ thin films.^{8–10}

II. EXPERIMENTAL DETAILS

The thin films of $\text{YBa}_2\text{Cu}_3\text{O}_{7-\delta}$ were prepared by laser ablation using a 308-nm XeCl excimer laser with a pulse energy density of 380 mJ in a partial pressure of 0.3 mbar of oxygen.⁵ The target used was high-density melt-textured stoichiometric $\text{YBa}_2\text{Cu}_3\text{O}_{7-\delta}$.¹¹ During deposition the (100) SrTiO_3 substrates were heated to a nominal temperature of 760° C, as measured using a thermocouple mounted in the heater block just behind the substrate. Measurements using an infrared pyrometer showed that the substrate surface was approximately 25° C lower than

this. After deposition the chamber pressure was raised to 1 atm of oxygen, the films were cooled to 470 °C, held there for 20 min to aid oxygenation, and then cooled to room temperature in approximately 20 min.

As-grown films prepared by this technique have T_c values ranging from 89 to 91 K and (10–90 %) transition widths typically of less than 1 K. The film thicknesses are typically 250 nm, within an estimated measurement error of $\pm 10\%$. For a film with T_c of 89 K, $\rho(300\text{ K}) = 240 \pm 20\ \mu\Omega\text{ cm}$ in good agreement with values quoted in the literature for twinned single crystals. The residual resistivities (defined by extrapolating the high-temperature linear resistivity to zero temperature) vary from essentially 0 to $20\ \mu\Omega\text{ cm}$. We attribute the differences to slight changes in the morphology of the films and possibly the incorporation of low levels of Si impurities out-gassed by the heaters, and use the extrapolated residual resistivity as a guide to quality. The films chosen for this study had residual resistivities of less than $10\ \mu\Omega\text{ cm}$ in their fully oxygenated state.

Our method for controlling the oxygen content was as follows. For a given value of δ , the samples were annealed in pure oxygen at a predetermined temperature, and then quenched, either on to a cooper block or into liquid nitrogen.¹² The annealing temperature was known approximately from earlier work on sintered $\text{YBa}_2\text{Cu}_3\text{O}_{7-\delta}$,² in which δ was measured from the weight loss and the value of δ for a given film was inferred from the measured T_c using the known relation² between T_c and δ . We found that, in general, our values of δ were higher than those of sintered material for identical annealing temperatures. For the bulk of this work ($\delta \leq 0.39$) only two films, which were deposited simultaneously, were used. At the end of the study one of these films was reoxygenated and the resistivity and transition temperature were found to be essentially unchanged from the “as-grown” sample.

In order to check the oxygen content of the films, we used electron probe microanalysis (EPMA) at the low accelerating voltage of 6.1 kV. At this voltage, the electron penetration into the sample is low (of the order of the film thickness), and by monitoring the emission from the Sr L_α x-ray line, it is possible to confirm that there is no significant electron penetration into the substrate. The thin film is then a bulk specimen from the point of view of EPMA, and the Y L_α , Ba L_α , Cu L_α , and O K_α x-ray emission from the film can be compared directly to those from a single-crystal standard. If the calculated oxygen content is to be expressed as a number of oxygen atoms per unit cell, uncertainties in the measured cation concentrations also contribute to the error, which can be estimated to correspond to an error in δ of ± 0.05 . Although this accuracy is not as good as that obtainable from weight loss measurements on sintered samples, we are not aware of any other technique that would allow such accurate oxygen analyses to be made nondestructively on thin films. Measured δ values are plotted as a function of the measured transition temperatures in Fig. 1, and are seen to be in agreement with the results from the sintered samples, within experimental error.

The films selected for transport measurements were

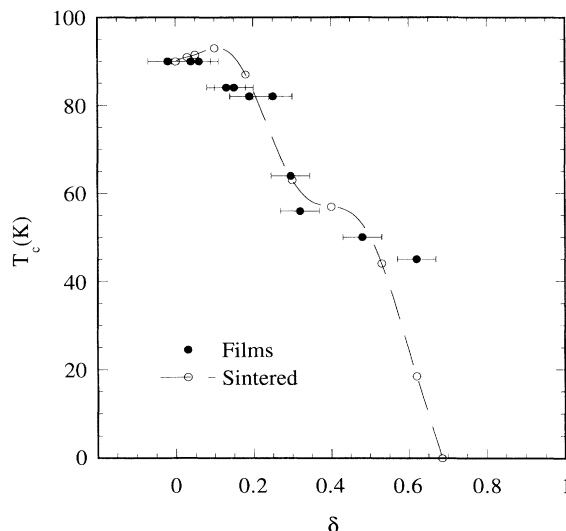


FIG. 1. Transition temperature (T_c) vs oxygen content (δ) for thin-film samples of $\text{YBa}_2\text{Cu}_3\text{O}_{7-\delta}$ and polycrystalline $\text{YBa}_2\text{Cu}_3\text{O}_{7-\delta}$ (Ref. 2). For the thin-film samples the values of δ were measured using electron probe microanalysis (EPMA), and for the sintered samples from weight loss.

patterned¹³ into bars 7 mm long by 0.5 mm wide. Current and voltage contacts were made to large contact pads, connected to the bar by tracks $30\ \mu\text{m}$ wide. The separation between the voltage contact points at the bar was 1.75 mm. The advantage of this kind of patterned geometry is that the separation of the voltage contacts is well controlled, and the ratio of the effective contact size to the contact separation is much better than can be achieved using conducting epoxy contacts to single crystals. The principal remaining uncertainty is the film thickness, and variations in thickness across the sample. EPMA measurements showed thickness differences of a few percent between two pairs of voltage contacts, which could also be monitored by observing the magnitude of the Hall voltage from the two contact pairs. The error in the absolute Hall coefficient and resistivity is dominated by the error (approximately 10–15 %) in the absolute thickness measurements of the films, but since this quantity cancels in the calculation of the Hall angle the error in this quantity is only $\pm 3\%$. Furthermore, since the two films used for the bulk of this work ($0.05 \leq \delta \leq 0.39$) were deposited simultaneously we expect their thicknesses and stoichiometry to be almost identical.

The resistivity was measured by a standard four-point, low-frequency ac (72 Hz) method, at a current density of $100\ \text{A cm}^{-2}$. The same frequency was used for Hall measurements and for each measurement point the sample was rotated by 180° in a fixed field (7 T) so that the small unbalanced resistive signal could be subtracted.

Data for two single crystals of $\text{YBa}_2\text{Cu}_3\text{O}_{7-\delta}$ ($\delta \approx 0.0$ and 0.4) grown in SnO_2 crucibles⁷ are also reported here. The annealing conditions for the crystals with $T_c = 90$ and 60 K were 1 week at 420°C in flowing O_2 and 1 week at 500°C in 1% O_2/N_2 , respectively. Small electrical contacts were then applied with silver epoxy (Dupont

6838), which after a short anneal (<15 min) under the same conditions as the original treatment, had a resistance of a few ohms.

III. RESULTS AND DISCUSSION

A. T_c

When deoxygenating samples it is essential that a uniform oxygen content is obtained throughout the sample. Our criterion for this was that the resistive transition remained sharp and Fig. 2 shows all samples up to and including $\delta=0.39$ had a FWHM in $d\rho/dT$ vs $T/T_c \leq 0.02$. We believe that the increase in transition width of the $\delta=0.53$ sample is a consequence of some inhomogeneity, together with the large increase in the slope of the T_c vs δ curve in this region of the phase diagram. In addition to the sharpness of the superconducting transition, EPMA analysis showed that the oxygen content, averaged over the e -beam spot size of $1 \mu\text{m}^2$, was homogeneous to within the detection limits (which correspond to ± 0.02 in δ).

B. Resistivity

The resistivity data are shown in Fig. 3. A striking difference between these data and those reported previously for sintered samples² (Fig. 4) is that the residual resistivity (ρ_{res}), as extrapolated from high temperatures, does not increase appreciably as δ increases. We ascribe this to a temperature-independent component in the resistivity of the sintered material that is probably caused by grain boundaries. It increases with δ either because the oxygen content is lower at the grain boundaries than in the bulk or because the resistivity of these interfaces strongly depends on the oxygen content, as does the c -axis resistivity.³ The observation that ρ_{res} remains low in

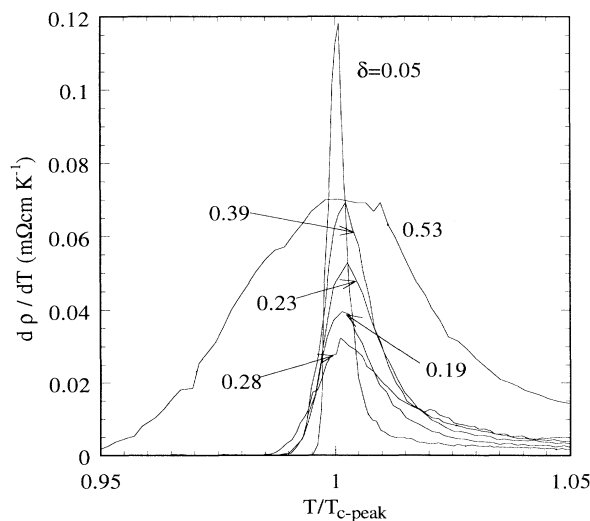


FIG. 2. $d\rho/dT$ vs $T/T_{c \text{ peak}}$ for the thin-film samples. $T_{c \text{ peak}}$ is the temperature of the maximum in $d\rho/dT$. The figure shows that the transition width remains sharp for $\delta \leq 0.39$.

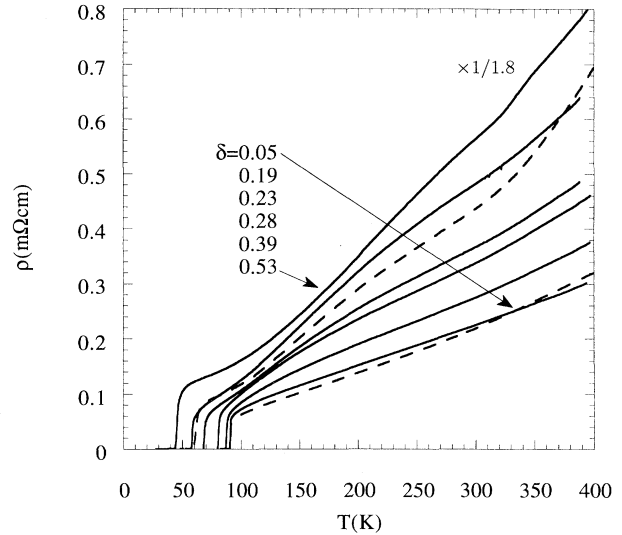


FIG. 3. ab -plane resistivity (ρ) vs temperature for thin-film samples of $\text{YBa}_2\text{Cu}_3\text{O}_{7-\delta}$ with $0.53 \leq \delta \leq 0.05$. Note the scale change for $\delta=0.53$. The dashed lines show $\rho(T)$ data for single crystals of $\text{YBa}_2\text{Cu}_3\text{O}_{7-\delta}$ with $\delta \approx 0.0$ and 0.4 .

the thin-film samples indicates that this is the intrinsic behavior of $\rho_{ab}(T)$ in oxygen-depleted $\text{YBa}_2\text{Cu}_3\text{O}_{7-\delta}$. It suggests that the main effect of introducing oxygen vacancies in the chain layer is to reduce the carrier concentration on the planes with no appreciable increase in scattering from the random defect potentials, except possibly for $\delta=0.53$. Figure 3 also shows $\rho(T)$ data for the two single crystals of $\text{YBa}_2\text{Cu}_3\text{O}_{7-\delta}$, which are very similar to the film data. This confirms that the film data reflect the intrinsic behavior of $\rho_{ab}(T)$.

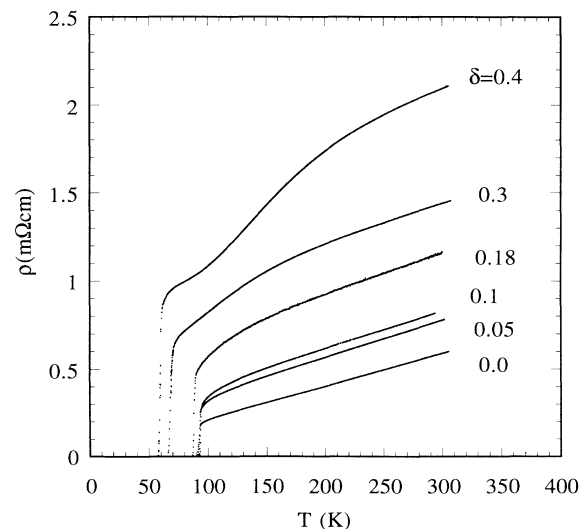


FIG. 4. Resistivity vs temperature for sintered samples of $\text{YBa}_2\text{Cu}_3\text{O}_{7-\delta}$ (Ref. 2). $\rho(T)$ is similar to that of the thin-film samples in Fig. 3, apart from a substantial increase in the residual resistivity of the sintered samples with δ .

As δ is increased (Fig. 3) there are considerable deviations from the linear behavior in $\rho(T)$ that is characteristic of the optimally doped material. Near room temperature, and below 320 K, $\rho(T)$ is roughly linear for all the samples, with a slope which increases by a factor 4.5 from $\delta=0$ to 0.53. As the temperature is lowered however, $\rho(T)$ develops considerable downward curvature. The reason for this behavior is not clear. In a previous analysis of oxygen-deficient $\text{YBa}_2\text{Cu}_3\text{O}_{7-\delta}$ with $0.18 \leq \delta \leq 0.0$, the curvature near T_c was analyzed in terms of superconducting fluctuations.² Near T_c the regular Aslamazov-Larkin (AL) term¹⁴ should dominate the fluctuation conductivity (σ_{fluc}), and the data of Ref. 2 for $\delta \approx 0$ could be understood using the AL formula applicable to three-dimensional fluctuations. Then as oxygen is removed the CuO layers become more decoupled² and the material becomes more two dimensional—thus causing an increase in the magnitude of σ_{fluc} . Further away from T_c the anomalous Maki-Thompson (MT) term¹⁵ may dominate. This term arises from the fact that superconducting fluctuations may cause a reduction in the normal electron-scattering rate. In principle it can be substantially larger than the AL term, especially in the presence of weak pair breaking and could possibly account for the downward curvature in Fig. 3. An alternative explanation may be found if one supposes that the resistivity in these compounds is primarily due to spin fluctuations.¹⁶ In this case and especially for larger values of δ , it may be possible to correlate the downward curvature in $\rho(T)$ with the properties of the spin excitation spectrum¹⁷ observed in neutron-scattering experiments.¹⁸

Fluctuation effects in $\text{YBa}_2\text{Cu}_3\text{O}_{7-\delta}$ thin films and crystals have been studied by a number of workers, for example, those of Refs. 19–24. The difficulty with fitting the observed resistivity to the fluctuation formulas is that the normal-state resistivity is not known precisely, and so any fits will depend on the choice of background. Bearing this in mind we tried two separate procedures to extract the fluctuation conductivity. First, it may be noted that $\rho(T)$ of the sample with $\delta=0.05$ is essentially linear from 150 to 320 K and that all the samples have a linear region around 300 K, the gradient of which increases monotonically with increasing δ . If this is assumed to be the intrinsic normal-state behavior the fluctuation conductivity may be deduced. For the more oxygen-deficient samples this procedure leads to very large values of σ_{fluc} near T_c . Fits to these data in the Ginzburg region ($1.01T_c - 1.1T_c$) were attempted with formulas including the two-dimensional AL and MT terms as given below:

$$\sigma_{\text{fluc}}^{\text{AL}} = \frac{e^2}{16\hbar d} \frac{1}{\tau}, \quad (2)$$

$$\sigma_{\text{fluc}}^{\text{MT}} = \frac{e^2}{8\hbar d} \frac{1}{\tau - \delta_{\text{pb}}} \ln \left[\frac{\tau}{\delta_{\text{pb}}} \right]. \quad (3)$$

Here τ is the reduced temperature [$\ln(T/T_c)$], d is the unit-cell parameter (11.7 Å) (assuming that the CuO_2 bilayers fluctuate as one unit), and δ_{pb} is a pair-breaking parameter. Figure 5 shows that for some values of δ the above formulas give reasonable fits to the data in the re-

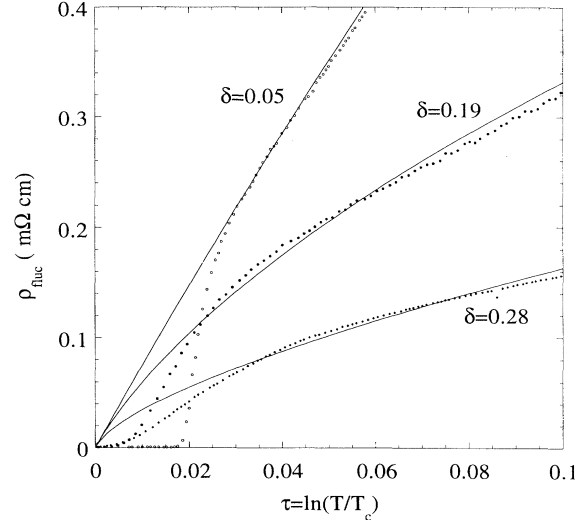


FIG. 5. The fluctuation resistivity extracted from the data in Fig. 3, after subtracting a linear normal-state resistivity fitted at high temperatures, plotted against reduced temperature [$\tau = \ln(T/T_c)$]. The fits shown are made using the Aslamazov-Larkin and Maki-Thompson formulas, Eqs. (2) and (3). The values of δ_{pb} used were 5, 0.22, and 0.025 for the films with δ (oxygen content) equal to 0.05, 0.19, and 0.28, respectively.

gion where $\rho_{\text{fluc}} \gtrsim \rho_{\text{tot}}$, and the perturbation treatment leading to Eqs. (2) and (3) can be expected to be valid. In order to account for the observed increase in fluctuation conductivity, however, δ_{pb} would have to decrease rapidly with increasing δ . While this may seem unlikely, it cannot be entirely ruled out at present because, for example, pair breaking could be the factor which limits T_c at high hole concentrations. It may be possible to check these values of δ_{pb} by precise measurements of the magnetoresistance above T_c in the fluctuation regime,^{21,23} but due to experimental constraints we have not attempted this here.

The second procedure is to assume that the nonlinearity of $\rho(T)$ at high temperatures is *not* due to superconducting fluctuations. The problem of determining the normal-state conductivity is then more difficult. A transparent way of seeing the effect of superconducting fluctuations on the resistivity is to subtract this extra conductivity from the measured values. The results of this procedure, which makes use of the fact that the 2D AL formula [Eq. (2)] has no adjustable parameters (except T_c), are shown in Fig. 6. Equation (2) was used for all samples except $\delta=0.05$ where the Lawrence-Doniach fluctuation formula,²⁵ which is applicable to layered superconductors, was used to fit the apparent 3D to 2D crossover observed at $1.008T_c$. This crossover temperature corresponds to a value for $\xi_c(0)$ of 1.1 Å which is in reasonable agreement with other work on fully oxygenated $\text{YBa}_2\text{Cu}_3\text{O}_{7-\delta}$ films and crystals,^{19–24} but lower than that found for ceramics.² Figure 6 shows that Eq. (2) provides a good description of the downward curvature immediately above T_c because the subtraction of the fluctuation conductivity given by Eq. (2) has linearized $\rho(T)$

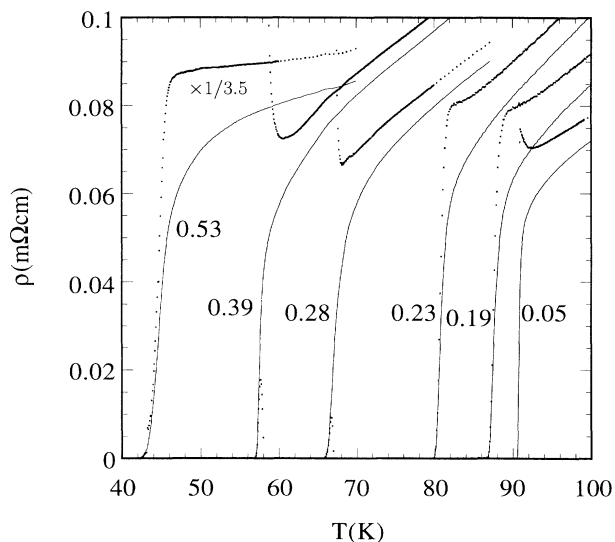


FIG. 6. The effect of the AL fluctuation conductivity on the resistivity data of Fig. 3. Equation (2) was used for all samples with $\delta \geq 0.19$ whereas for the $\delta = 0.05$ sample the Lawrence-Doniach formula (Ref. 25) for layered superconductors was used (with a c -axis coherence length $\xi_0 = 1.1$ Å). The original data are shown by thin lines and the corrected data by symbols. The T_c values used in the AL formulas correspond approximately to the 50% transition points.

in this region. The sample for which the fit is worst ($\delta = 0.39$) has a small resistive anomaly at 68 K which may be indicative of some inhomogeneity.

C. Hall effect

The behavior of the Hall coefficient as a function of temperature remains one of the most intriguing and controversial normal-state properties of oxide superconductors.²⁶ For the optimally doped material the inverse Hall coefficient ($1/R_H$) decreases linearly with temperature. At other doping levels there are significant deviations from this simple behavior.^{7,27} It has been suggested⁶ that a more appropriate quantity for the analysis of Hall data is the inverse Hall angle ($\cot \Theta_H = \rho / \rho_{xy}$), where $\rho_{xy} = (R_H B)$ is the Hall resistivity and B is the magnetic field. Experimental data presented here and elsewhere^{7,27,28} show that $\cot \Theta_H$ retains its predominantly T^2 temperature dependence while the temperature dependences of $\rho(T)$ and $R_H(T)$ change systematically across the full doping range.

Hall coefficient data corresponding to the resistivities in Fig. 3 are shown in Fig. 7. The strong increase in R_H with increasing δ is often ascribed to a decrease in the carrier concentration (n), although in one picture proposed recently^{7,17} it arises from changes in the anisotropy of the mean free path over the Fermi surface, rather than changes in n itself. One feature of all the data in Fig. 7 is the maximum in R_H in the normal state that broadens and shifts to higher temperature as δ is increased. This anomaly has been ascribed either to superconducting

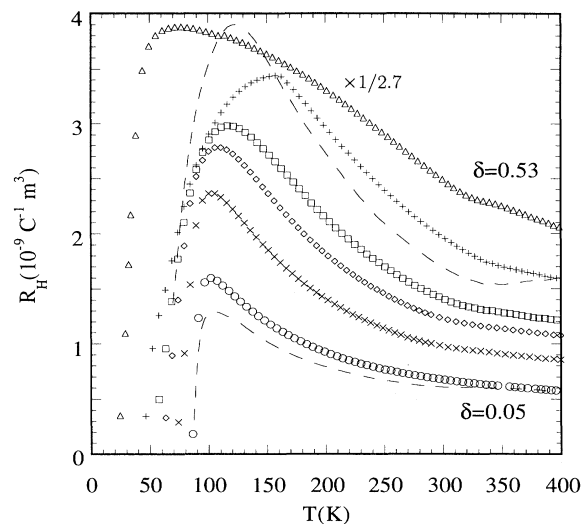


FIG. 7. ab -plane Hall coefficient (R_H) corresponding to the resistivities in Fig. 3. The measurement field was 7 T. For convenience the data for the $\delta = 0.53$ sample have been divided by 2.7. The dashed lines show data for two single crystals of $\text{YBa}_2\text{Cu}_3\text{O}_{7-\delta}$ with $\delta \approx 0.0$ and 0.4.

fluctuations as in $\text{YBa}_2\text{Cu}_3\text{O}_7$ (Ref. 24) or to a property of the normal state as in 2201 BiSCO .²⁹ For the present case we tend to favor the former viewpoint because R_H falls continuously as T_c is approached, but we have not been able to obtain good fits to standard fluctuation formulas.³⁰ Above these maxima $1/R_H$ increases approximately linearly with T and then above 300 K either flattens off or shows an abrupt change in slope (Fig. 8).

In Fig. 9, the R_H data in Fig. 7 are replotted as $\cot \Theta_H$ vs T^2 for comparison with Eq. (1). Despite the large

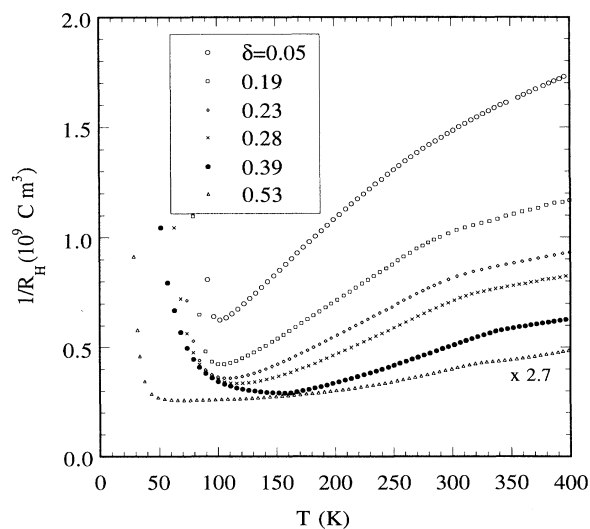


FIG. 8. Inverse Hall coefficient ($1/R_H$), corresponding to the data in Fig. 7. The data for the $\delta = 0.53$ sample have been multiplied by 2.7.

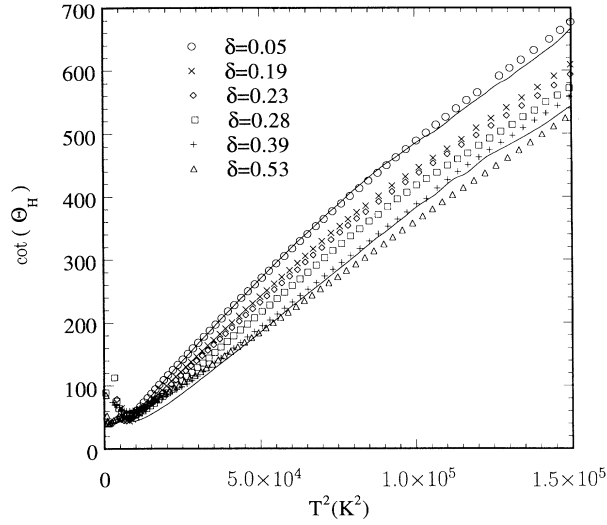


FIG. 9. Inverse Hall angle ($\cot\Theta_H$) calculated from the data in Figs. 3 and 7. The gradient of the T^2 plot decreases as δ is increased. As in Fig. 7 the solid lines show data for two single crystals of $\text{YBa}_2\text{Cu}_3\text{O}_{7-\delta}$.

changes in $\rho(T)$ and $R_H(T)$ with δ (Figs. 3 and 7), there are only minor changes in $\cot\Theta_H$. The gradient of the T^2 plot (A) decreases monotonically with δ (Fig. 10) whereas the zero-temperature intercept (B) remains approximately constant (in all cases the gradient was obtained from the region where the data were best described by the T^2 law as discussed in Sec. III D). We note that the behavior displayed here for both our single-crystal and thin-film samples (A falling as T_c is

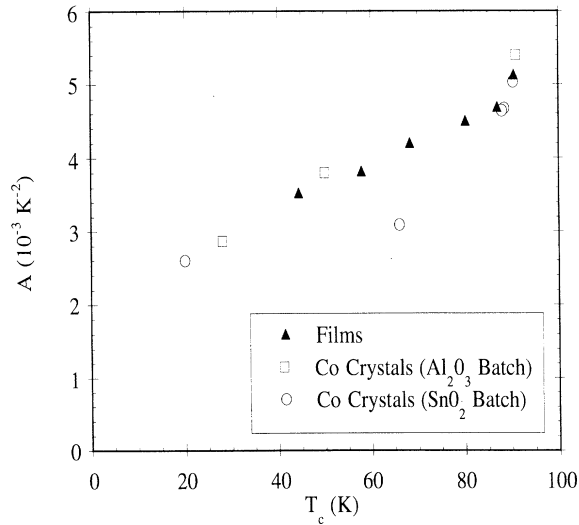


FIG. 10. The gradient of $\cot\Theta_H(T^2)$ for thin films of $\text{YBa}_2\text{Cu}_3\text{O}_{7-\delta}$ and single-crystal $\text{YBa}_2(\text{Cu}_{1-x}\text{Co}_x)_3\text{O}_{7-\delta}$ grown in SnO_2 and Al_2O_3 crucibles (Ref. 7). In all cases the fits were made in the linear region of the $\cot\Theta_H(T^2)$ plot (see Sec. III D, i.e., at lower temperatures for smaller values of δ , etc.).

duced by underdoping), is consistent with that found previously for single crystals of $\text{YBa}_2(\text{Cu}_{1-x}\text{Co}_x)_3\text{O}_{7-\delta}$,⁷ and recent work on low resistivity films⁸ but not with some other single-crystal measurements³¹ and films with higher residual resistivities.¹⁰ Within the Anderson picture^{6,28} a decrease in A corresponds to an increase in spinon bandwidth, as discussed previously,⁷ whereas in a more traditional approach^{7,17} it reflects changes in the anisotropy of the mean free path over the Fermi surface.

D. Deviations from simple power-law behavior

Although the $\cot\Theta_H$ data of Fig. 9 are in broad agreement with Eq. (1), there are deviations from this law at both high and low temperatures. For $\delta=0.05$ the slope of the T^2 plot falls smoothly between 200 and 300 K, while for the other samples it changes more abruptly. Related features can be seen in the high-temperature resistivity data and have been observed by other workers.^{31,32} The origin of these anomalies is not clear, but it is possible that they are connected with oxygen ordering phenomena in the CuO chains because the size of the resistivity anomaly increases with δ but disappears completely upon addition of impurity atoms such as Al or Co in the CuO chains.⁷ The overall behavior of the data is that for low δ there is a decrease in the slope of $\cot\Theta_H(T^2)$ at the temperature where $d\rho/dT$ increases. However, the anomaly in $\rho(T)$ becomes larger as δ is increased, while that in $\cot\Theta_H$ becomes smaller. In fact, the sample with the largest anomaly in $\rho(T)$ ($\delta=0.53$) shows almost no corresponding feature in $\cot\Theta_H(T^2)$.

The nonlinearities in $\cot\Theta_H(T^2)$ that occur at low temperature (<150 K) for the samples with high δ (0.39, 0.53) may be caused by localization effects but alternatively within the approach of Ref. 17, they also could reflect changes in the relative strength of the spin fluctuation and electron-electron scattering.

E. Magnetoresistance

The resistive transitions of the films were studied in fields of up to 7 T, applied parallel to the crystallographic a - b or c axes. Temperatures were measured using a carbon glass thermometer which has little magnetoresistance in the field range considered. For B parallel to a - b , the film was aligned with the field to within $\pm 1^\circ$ by searching for the minimum in resistance at a temperature approximately halfway down the transition. For the sample with $\delta=0.05$, the resistivity was independent of current [at the current densities (~ 100 A cm⁻²) used in this study] for at least 3 orders of magnitude below the normal state. The raw data in Fig. 11 clearly show that for $B\parallel c$ oxygen depletion leads to a strong monotonic increase in the field broadening with δ . This increase is less marked for $B\perp c$ but as mentioned below it is still appreciable on a suitably normalized temperature scale. Arrhenius plots of $\ln\rho$ vs $1000/T$ are shown in Fig. 12. It can be seen that, except possibly at the lowest temperatures, the data in Fig. 12 cannot be described by a single activation energy. It might be possible to understand these data in terms of

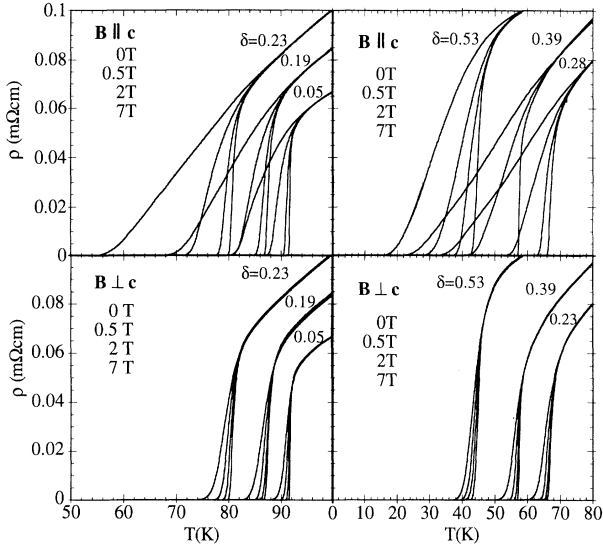


FIG. 11. Magnetoresistance data for thin films of $\text{YBa}_2\text{Cu}_3\text{O}_{7-\delta}$ near T_c . The top two panels show resistance vs temperature for B parallel to c and the bottom two for B perpendicular to c . The fields and δ values are indicated in the figure. The current was in the ab plane in all cases. For $\delta=0.39$ there are no data for $B=0.5\text{ T}$, applied parallel to c .

thermally activated flux motion as in the work of Zhu *et al.*³³ This will be attempted later when I - V measurements are available to fix some of the parameters.³³ In all cases the resistivity falls continuously to zero with no obvious discontinuity that could define a “transition temperature” or $B_{c2}(T)$ line. However, if the logarithm of the resistance is plotted against temperature (not shown) the resistance is seen to fall sharply when it has reached approximately 0.1% of its normal-state value. We define this temperature as $T^*(B)$, and in Fig. 13 we plot the ratio $T^*(B)/T^*(0)$ vs applied field (B). This is a transparent way of showing that the transition broadens considerably as δ is increased. Figures 13(a) and 13(b) seem to show that both field orientations ($B \perp c$ and $B \parallel c$) give similar results, albeit on a different temperature scale. For conventional low- T_c type-II superconductors, Fig. 13 would show how the upper critical field B_{c2} varies with temperature, and since κ , the Ginzburg-Landau parameter, only varies by $\sim 20\%$,³⁴ it should approximately follow the quadratic behavior of the thermodynamic critical field (B_c). It can be seen that, for our data, the curvature of $B(T)$ is of the wrong sign to allow this simple interpretation. Interpretations of the transition in terms of standard flux-flow models may be incomplete because they do not explain the weak dependence of the resistance on the relative orientation of the field and current directions (i.e., the virtual absence of a Lorentz force dependence of the resistivity).^{35,36} However, if all the curves in Fig. 13(a) ($B \parallel c$) are normalized by a suitably chosen scaling field $B^*(0)$ (Fig. 14) they fall on to a single universal curve, the form of which is approximated well by the relation

$$B^*(T) = B^*(0) \left[1 - \left(\frac{T^*(B)}{T^*(0)} \right) \right]^{4/3}. \quad (4)$$

This scaling was also obtained for $B \perp c$ (not shown) but here an exponent of $\frac{3}{2}$ was a better fit to the data. The above particular power law is expected for critical fluctuations which are described by the 3D XY model,^{37–39} analogous to those observed at the λ point of superfluid He^4 , e.g., Ref. 38. As shown in Fig. 14, Eq. (4) seems to hold over most of the field and temperature range studied here. It is not clear to us whether this power law actually represents the upper critical field $B_{c2}(T)$ itself, in the limit where the critical region is broad, as in the treatment of Ref. 38, or whether it represents the vortex lattice melting line expected at $\sim 0.1B_{c2}$.^{37,39} In either event, applica-

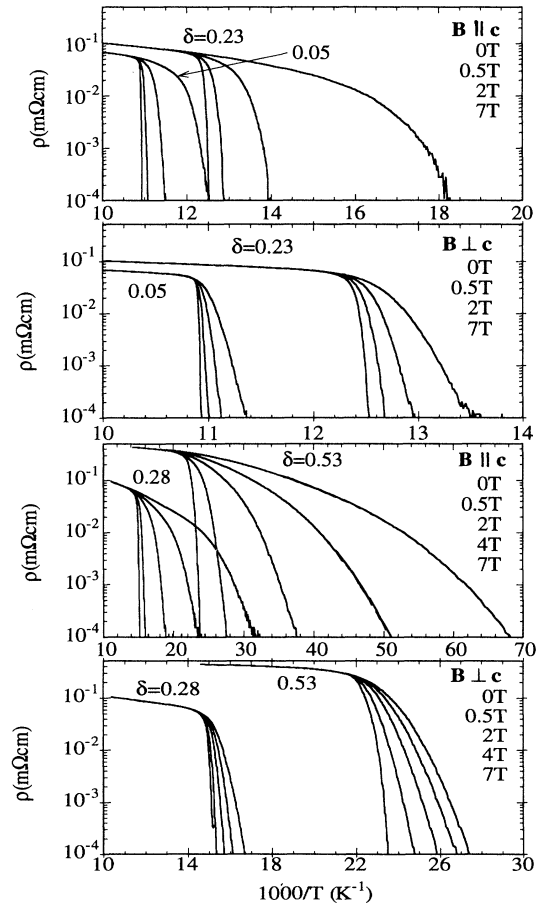


FIG. 12. Arrhenius plots [$\ln(\rho)$ vs $1000/T$], showing the broadening of the resistive transition for thin films of $\text{YBa}_2\text{Cu}_3\text{O}_{7-\delta}$. The top two panels show data for $\delta=0.05$ and 0.23 , in fields of 0, 0.5, 2, and 7 T, applied parallel to c (first panel) and perpendicular to c (second panel). The bottom two panels show data for $\delta=0.28$ and 0.53 in fields of 0, 0.5, 2, 4, and 7 T, applied parallel to c (third panel) and perpendicular to c (fourth panel). The current is in the ab plane in all cases.

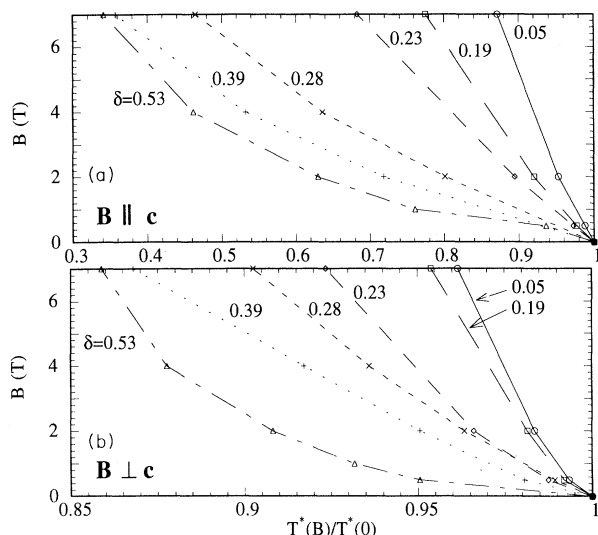


FIG. 13. Field (B) vs $T^*(B)/T^*(0)$ (defined in text) with (a) B perpendicular to the ab plane, (b) B parallel to the ab plane.

tion of a magnetic field along the c axis of $\text{YBa}_2\text{Cu}_3\text{O}_{7-\delta}$ seems to broaden the critical region substantially. Since the $B^*(0)$ values fall sharply with δ , it is also broadened by oxygen depletion. A somewhat different picture has been proposed recently to account for the field-induced broadening of $\text{Bi}_2\text{Sr}_2\text{CaCu}_2\text{O}_{8+\delta}$ films⁴⁰ and $\text{Bi}_{1.7}\text{Pb}_{0.3}\text{Sr}_{1.9}\text{CaCu}_{1.9}\text{O}_{8+\delta}$ crystals.⁴¹ In this case the giant fluctuations are attributed to decoupling of the superconducting CuO_2 layers by a magnetic field, rather than 3D XY behavior. More detailed studies of the present films to higher magnetic fields may help to clarify the relationship between these two approaches.

IV. CONCLUSIONS

In summary we have made a systematic study of the effect of oxygen depletion on the ab -plane resistivity, Hall effect, and magnetoresistance of laser ablated $\text{YBa}_2\text{Cu}_3\text{O}_{7-\delta}$ films. We have obtained some unexpected

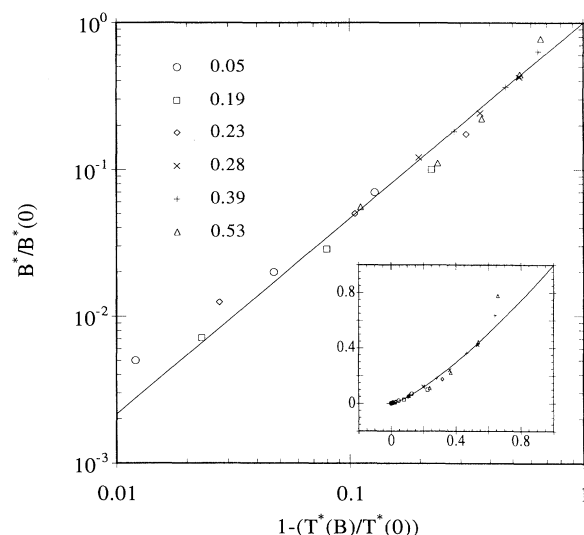


FIG. 14. Reduced field $B^*/B^*(0)$ vs $T^*(H)/T^*(0)$ (defined in text) for $0 \leq B \leq 7$ T applied perpendicular to the ab plane. The scaling fields $B^*(0)$ are 100, 70, 40, 16.5, 11, and 9 T for δ values of 0.05, 0.19, 0.23, 0.28, 0.39, and 0.53, respectively. The solid curve is Eq. (4) showing the power-law dependence. The inset shows the same data plotted on linear axes.

results especially with regard to the low residual resistivities, the strong curvature in $\rho(T)$, the relatively small variation in inverse Hall angle with δ , and the $\frac{4}{3}$ -power-law behavior of the scaled magnetic fields.

ACKNOWLEDGMENTS

We would like to thank K. Scott and W. A. Phillips for originally setting up the laser ablation apparatus, P. S. I. P. N. De Silva for assistance in preparing oxygen-deficient $\text{YBa}_2\text{Cu}_3\text{O}_{7-\delta}$ crystals, and J. W. Loram, W. Y. Liang, and M. A. Howson for helpful discussions. We gratefully acknowledge partial support of the laser ablation project by GEC.

*On leave from the Institute of Physics of the University, Zagreb, Croatia.

¹J. W. Loram, J. R. Cooper, and K. A. Mirza, *Supercon. Sci. Tech.* **4**, S391 (1991).

²J. R. Cooper, S. D. Obertelli, A. Carrington, and J. W. Loram, *Phys. Rev. B* **44**, 12 086 (1991).

³T. Ito, H. Takagi, S. Ishibashi, T. Ido, and S. Uchida, *Nature* **350**, 596 (1991).

⁴S. J. Rothman, J. L. Routbort, U. Welp, and J. E. Baker, *Phys. Rev. B* **44**, 2326 (1991).

⁵K. Scott, PhD. thesis, Cambridge University, 1992.

⁶P. W. Anderson, *Phys. Rev. Lett.* **67**, 2092 (1991).

⁷A. Carrington, A. P. Mackenzie, C. T. Lin, and J. R. Cooper, *Phys. Rev. Lett.* **69**, 2855 (1992).

⁸B. Wuyts, E. Osquiguil, M. Maenhoudt, S. Libbrecht, Z. X. Gao, and Y. Bruynseraede, *Phys. Rev. B* **47**, 5512 (1993).

⁹E. C. Jones, D. K. Christen, J. R. Thompson, R. Feenstra, S.

Zhu, D. H. Lowndes, J. M. Philips, M. P. Siegal, and J. D. Budai, *Phys. Rev. B* **47**, 8986 (1993).

¹⁰P. Xiong, G. Xiao, and X. D. Wu, *Phys. Rev. B* **47**, 5516 (1993).

¹¹We would like to thank N. Alford of ICI Advanced Materials for our high-density $\text{YBa}_2\text{Cu}_3\text{O}_{7-\delta}$ targets.

¹²The quench temperatures (and values of δ) were as follows: 535°C (0.19), 570°C (0.23), 610°C (0.28), 650°C (0.39), and 650°C (0.53). The final quench ($\delta=0.53$) was into liquid nitrogen whereas in other cases the samples were quenched directly on to a copper block.

¹³The films were patterned using a photolithographic technique with an EDTA etch.

¹⁴L. G. Aslamazov and A. I. Larkin, *Phys. Lett.* **27A**, 117 (1968).

¹⁵K. Maki, *Prog. Theor. Phys.* **39**, 897 (1968).

¹⁶T. Moriya, Y. Takahashi, and K. Ueda, *J. Phys. Soc. Jpn.* **59**,

- 2905 (1990).
- ¹⁷J. R. Cooper and A. Carrington, *Proceedings of the Fifth International Symposium on Superconductivity*, Kobe, Japan (Springer-Verlag, Berlin, 1992).
- ¹⁸J. Rossat-Mignod, L. P. Regnault, C. Vettier, P. Bourges, P. Burlat, J. Bossy, J. Y. Henry, and G. Lapertot, *Physica C* **185-189**, 86 (1991).
- ¹⁹C. Baraduc, V. Pagnon, A. Buzdin, J. Y. Henry, and C. Ayache, *Phys. Lett. A* **166**, 267 (1992).
- ²⁰R. Hopfengärtner, B. Hensel, and G. Saemann-Ischenko, *Phys. Rev. B* **44**, 741 (1991).
- ²¹N. Overend and M. A. Howson, *J. Phys. C* **4**, 9615 (1992).
- ²²V. Pagnon, C. Villard, C. Ayache, and J. C. Villegier, *Physica B* **169**, 645 (1991).
- ²³Y. Matsuda, T. Hirai, S. Komiyama, T. Terashima, Y. Bando, K. Iijima, K. Yamamoto, and K. Hirata, *Phys. Rev. B* **40**, 5176 (1989).
- ²⁴J. P. Rice, J. Giapintzakis, D. M. Ginsberg, and J. M. Mochel, *Phys. Rev. B* **44**, 10 158 (1991).
- ²⁵W. E. Lawrence and S. Doniach, in *Proceedings of the Twelfth International Conference on Low-Temperature Physics, Kyoto* (Keigaku, Tokyo, 1970).
- ²⁶Y. Iye, in *Physical Properties of High Temperature Superconductors III*, edited by D. M. Ginsberg (World Scientific, Singapore, 1992).
- ²⁷Y. Kubo, Y. Shimakawa, T. Manako, and H. Igarashi, *Phys. Rev. B* **43**, 7875 (1991).
- ²⁸T. R. Chien, Z. Z. Wang, and N. P. Ong, *Phys. Rev. Lett.* **67**, 2088 (1991).
- ²⁹A. P. Mackenzie, S. D. Hughes, J. R. Cooper, A. Carrington, C. Chen, and B. M. Wanklyn, *Phys. Rev. B* **45**, 527 (1992).
- ³⁰H. Fukuyama, H. Ebisawa, and T. Tsuzuki, *Prog. Theor. Phys.* **46**, 1028 (1971).
- ³¹J. M. Harris, Y. F. Yan, and N. P. Ong, *Phys. Rev. B* **46**, 14 293 (1992).
- ³²T. R. Chien, D. A. Brawner, Z. Z. Wang, and N. P. Ong, *Phys. Rev. B* **43**, 6242 (1991).
- ³³S. Zhu, D. K. Christen, C. E. Klabunde, J. R. Thompson, E. C. Jones, R. Feenstra, D. H. Lowndes, and D. P. Norton, *Phys. Rev. B* **46**, 5576 (1992).
- ³⁴E. Helfand and N. R. Werthamer, *Phys. Rev.* **147**, 288 (1966).
- ³⁵S. Kambe, M. Naito, K. Kitazawa, I. Tanaka, and H. Kojima, *Physica C* **160**, 243 (1989).
- ³⁶J. N. Li, K. Kadowski, M. J. V. Menken, A. A. Menovsky, and J. J. M. Franse, *Physica C* **161**, 313 (1989).
- ³⁷D. S. Fisher, M. P. A. Fisher, and D. A. Huse, *Phys. Rev. B* **43**, 130 (1991).
- ³⁸L. N. Bulaevskii, V. L. Ginzburg, and A. A. Sobyenin, *Zh. Eksp. Teor. Fiz.* **94**, 355 (1988) [*Sov. Phys. JETP* **67**, 1499 (1988)].
- ³⁹M. B. Salamon, J. Shi, N. Overend, and M. A. Howson, *Phys. Rev. B* **47**, 5520 (1993).
- ⁴⁰H. Raffy, S. Labdi, O. Laborde, and P. Monceau, *Physica C* **184**, 159 (1991).
- ⁴¹C. M. Fu, W. Boon, Y. S. Wang, V. V. Moshchalkov, and Y. Bruynseraede, *Physica C* **200**, 17 (1992).